

Spectroscopy and photometry of multiple populations along the asymptotic-giant branch of NGC 2808 and NGC 6121 (M 4) ¹

A. F. Marino², A. P. Milone², D. Yong², G. Da Costa², M. Asplund², L. R. Bedin³, H. Jerjen², D. Nardiello⁴, G. Piotto^{3,4}, A. Renzini³, M. Shetrone⁵

ABSTRACT

We present a photometric and spectroscopic study of multiple populations along the asymptotic-giant branch (AGB) of the intermediate-metallicity globular clusters (GCs) NGC 2808 and NGC 6121 (M 4). Chemical abundances of O, Na, Mg, Al, Si, Ca, Sc, Ti, V, Cr, Fe, Co, Ni, Zn, Y, and Ce in AGB stars from high-resolution FLAMES+UVES@VLT spectra are reported for both clusters. Our spectroscopic results have been combined with multi-wavelength photometry from the *HST* UV survey of Galactic GCs and ground-based photometry, plus proper motions derived by combining stellar positions from ground-based images and Gaia DR1. Our analysis reveals that the AGBs of both clusters host multiple populations with different chemical composition.

In M 4 we have identified two main populations of stars with different Na/O content, lying on distinct AGBs in the m_{F438W} vs. $C_{F275W,F336W,F438W}$ and the V vs. $C_{U,B,I}$ pseudo-CMDs.

In the more massive and complex GC NGC 2808 three groups of stars with different chemical abundances occupy different locations on the so-called "chromosome map" photometric diagram. The spectroscopic+photometric comparison of stellar populations along the AGB and the red giants of this GC suggests that the AGB hosts stellar populations with a range in helium abundances spanning from primordial up to high contents of $Y \sim 0.32$. On the other hand, from our dataset, there is no evidence for stars with extreme helium abundance ($Y \sim 0.38$)

²Research School of Astronomy & Astrophysics, Australian National University, Canberra, ACT 2611, Australia

³Istituto Nazionale di Astrofisica - Osservatorio Astronomico di Padova, Vicolo dell'Osservatorio 5, Padova, IT-35122

⁴Dipartimento di Fisica e Astronomia 'Galileo Galilei' - Univ. di Padova, Vicolo dell'Osservatorio 3, Padova, IT-35122

⁵McDonald Observatory, The University of Texas at Austin, 1 University Station, C1400, Austin, TX 78712-0259, USA

on the AGB, suggesting that the most He-rich stars of NGC 2808 do not reach this phase.

Subject headings: globular clusters: individual (NGC 2808, NGC 6121) — chemical abundances – Population II – Hertzsprung-Russell diagram

1. Introduction

It is now established that virtually all Galactic Globular Clusters (GCs) host two or more stellar populations with different chemical composition: a first population of stars with the same chemical abundance as halo field stars at similar metallicity, and second population(s) of stars enhanced in helium, nitrogen, and sodium and depleted in carbon and oxygen (e.g. Kraft 1994; Gratton et al. 2012). In the last decade, multiple stellar populations have been homogeneously studied in a large number of Galactic GCs by using both spectroscopy and photometry (e.g. Carretta et al. 2009; Piotto et al. 2015; Milone et al. 2017 and references therein). Most of these studies focused on stars along the red-giant branch (RGB), the sub-giant branch, and the main sequence (MS). Little attention, however, has been devoted to more evolved stages, like the asymptotic-giant branch (AGB).

Spectroscopic work has shown that AGB stars of the few studied GCs can exhibit star-to-star variation in light elements, in analogy with what is observed along the RGB. These conclusions are based both on early analysis of molecular bands (e.g. Smith & Norris 1993) and, more recently, on high-resolution spectroscopy of light elements (e.g. Ivans et al. 1999, 2001; Johnson et al. 2015).

On the photometric side, appropriate combination of ultraviolet and optical filters of the *Hubble Space Telescope* (*HST*), such as the $C_{F275W,F336W,F438W} = (m_{F275W} - m_{F336W}) - (m_{F336W} - m_{F438W})$ pseudo-color, have been proved to provide a powerful means to identify multiple populations along the entire color-magnitude diagram (CMD) of GCs, from the MS up to the RGB and the horizontal-branch (Milone et al. 2013). Recent work has then used this index to investigate the AGB, and found that the AGB of NGC 2808 hosts three distinct sequences (Milone et al. 2015a). Similarly, the AGBs of the GCs NGC 7089 and NGC 6352 are found to be inconsistent with a simple stellar population (Milone et al. 2015b; Nardiello et al. 2015a; for further photometric evidence see Gruyters et al. 2017).

¹Based on observations with the NASA/ESA *Hubble Space Telescope*, obtained at the Space Telescope Science Institute, which is operated by AURA, Inc., under NASA contract NAS 5-26555.

On the other hand, there is some evidence that the population ratio, in terms of light elements chemical abundances, is different among RGB and AGB stars. Early analysis on cyanogen (CN) band strengths by Smith & Norris (1993) found a different distribution of CN-band strengths among AGBs and RGBs in NGC 6752 and M 5. More recently, a lack of AGB stars with the highest sodium abundance observed on the RGB has been shown for NGC 6752 and NGC 6266 (M 62, Campbell et al. 2013; Lapenna et al. 2015, 2016). In 47 Tuc, the AGB displays similar Na abundance variations as in the RGB, but a fraction of $\lesssim 20\%$ of Na-rich RGB stars may not reach the AGB phase (Johnson et al. 2015). These results suggest that some stars enriched in the high temperature H-burning products fail to ascend the AGB and have raised new interest in stellar populations in this evolutionary phase.

As the chemical enrichment in Na is indicative for a star to belong to a second stellar population in GCs, this means that the AGBs of some GCs may display a paucity of second population stars compared to the RGB. Qualitatively, enrichment in helium among second population stars, as observed in GCs (e.g. Milone et al. 2014), can account for the lack of the Na (and He)-richest stars along the AGB. Indeed, He-enhanced stars have smaller envelope masses (and higher surface temperature) on the horizontal branch, and, if the mass is low enough, they evolve directly to the white dwarf sequence through the so-called ‘AGB-manque’ phase. The lack of AGB stars in M 62 is consistent with this scenario as the populous second-generation of this cluster has extremely high helium abundance ($Y \sim 0.33$, Milone 2015). Quantitatively, most GCs have internal helium variations, $\Delta(Y)$, of just a few hundredths (Milone 2015). Evolution models of low-mass stars suggest that, besides helium, the maximum sodium content expected on the AGB is a function of both metallicity and age, as with younger ages stars are more massive on the horizontal branch hence will have a better chance to climb the AGB even if helium rich (e.g., Charbonnel & Chanterau 2016).

In this paper we combine multi-wavelength photometry from *HST* and ground-based telescopes with high-resolution spectroscopy from the Ultraviolet and Visual Echelle Spectrograph (UVES, Dekker et al. 2000) of the Very Large Telescope (VLT) to further investigate the multiple populations along the AGB of the mildly metal-poor GCs NGC 2808 and NGC 6121 (M 4).

The targets of this paper, NGC 2808 and M 4, have been widely investigated in the context of multiple populations. NGC 2808 is one of the most massive and complex GCs of the Milky Way. Its ‘chromosome map’, a photometric diagram introduced by Milone et al. (2015a) to separate different stellar groups in GCs, hosts at least five distinct populations (e.g. Milone et al. 2015a; Carretta 2015). It exhibits stellar populations with very-high helium content ($Y \sim 0.32$ and $Y \sim 0.38$, D’Antona et al. 2005; Piotto et al. 2007; Marino et al. 2014) and extreme variations in light element abundances, including O, Mg, Al, Si, and

Na (Carretta et al. 2009; Carretta 2014).

In contrast, M 4 is a much simpler GC. It hosts “only” two main populations (Marino et al. 2008; Lee et al. 2009; Milone et al. 2014, 2017) with relatively small variations in light elements (Ivans et al. 1999; Marino et al. 2008, 2011; Carretta et al. 2009; Villanova et al. 2011) and helium ($\Delta Y \sim 0.02$, Villanova et al. 2012; Nardiello et al. 2015b) compared to NGC 2808.

The AGBs of both NGC 2808 and M 4 have been recently investigated by means of high-resolution spectroscopy. Wang et al. (2016) has determined the sodium abundance of 31 AGB stars in NGC 2808 and concluded that this cluster hosts second-generation AGB stars and that the fraction of Na-rich AGB stars is *higher* than that observed on the RGB.

The presence of multiple populations along the AGB of M 4 is a quite controversial issue. The chemical composition of 15 AGB stars in M 4 has been recently investigated by MacLean et al. (2016) using the 2dF+HERMES facility on the Anglo-Australian Telescope. These authors have suggested that the AGB is mostly populated by stars with low sodium and high oxygen abundance. However, these findings have been photometrically challenged by the recent work of Lardo et al. (2017) who have analyzed the V vs. $C_{U,B,I} = (U - I) - (B - I)$ diagram of M 4 and concluded that its broadened AGB is not consistent with a simple population.

The layout of the paper is as follows: Sect. 2 presents the photometric and spectroscopic data that we have analysed; our chemical analysis is described in Sect. 3; our results on chemical abundances of AGB stars are discussed in Sect. 4 in conjunction with the photometric properties; finally Sect. 5 is a summary of our results.

2. Observations and data reduction

In order to study multiple stellar populations along the AGB of M 4 and NGC 2808 we have combined information from both photometry and spectroscopy. The photometric and spectroscopic datasets will be described in the following subsections.

2.1. The photometric dataset and target selection

We have used both *HST* and ground-based photometry of NGC 2808 and M 4. The photometric and astrometric catalogs from *HST* have been published by Piotto et al. (2015) and include stars in the innermost ($\sim 2.7' \times 2.7'$) clusters regions. They have been derived from images collected through the $F275W$, $F336W$, $F438W$ filters of the Ultraviolet and

Visual Channel of the Wide Field Camera 3 (UVIS/WFC3) on *HST*. The data include stellar proper motions. Moreover, they also provide photometry of images from Anderson et al. (2008), collected with the F814W band of the Wide Field Channel of the Advanced Camera for Survey on *HST*. Only stars that, according to their proper motions, are considered cluster members are included in the analysis. This photometric dataset has been used in several works (Piotto et al. 2015; Milone et al. 2015a, 2017; Simioni et al. 2016) to investigate stellar populations in NGC 2808 and M 4 and we refer the reader to these papers for further details on the data and the data reduction.

In addition, we have used the wide-field photometric catalogs from the database maintained by Peter Stetson which are derived from images collected with ground-based facilities (see Stetson 1987, 1994, 2000; Stetson et al. 2014). These data have been previously used by Monelli et al. (2013) to study multiple stellar populations along the RGB of both M 4 and NGC 2808. We refer the reader to these papers for details on the dataset and on the method used to derive the photometry and astrometry. We have calculated relative proper motions by combining the positions of stars derived from images collected with the Wide Field Imager (WFI) of the MPI 2.2m telescope in La Silla with those from the Gaia data release 1 (Lindegren et al. 2016).

The WFI data used to calculate stellar proper motions in the field of M 4 consist of $6 \times 100s + 3 \times 10s$ images collected on June 18th and 21th, 2001 through the *B* band (program 69.D-05282). Photometry and astrometry of these images have been computed using the programs from Anderson et al. (2006) while proper motions have been derived as in Anderson et al. (2006) and Piotto et al. (2012). Both *HST* and ground-based photometry has been corrected for differential reddening following the recipe by Milone et al. (2012).

The CMDs of stars in the field of view of M 4 and NGC 2808 from ground-based and *HST* photometry are shown in Fig. 1 and Fig. 2, where we indicate with orange diamonds our sample of seventeen and seven spectroscopically-analysed AGB stars, respectively. The remaining AGB stars have been studied from photometry only, and are represented with black diamonds. We also show the vector point diagram of proper motions obtained by combining the coordinates of stars from the Gaia and WFI catalogs, that has been used to identify candidate cluster members and field stars. Our target AGB stars were carefully selected from CMDs derived from both the ground-based and *HST* observations. Specifically, for NGC 2808 we have selected three stars on the three main AGB sequences identified by Milone et al. (2015a) by using the $C_{F275W, F336W, F438W}$ index from *HST* photometry. The remaining four stars of NGC 2808 have been selected from ground-based photometry by Stetson (2000). In the case of M 4, multi-wavelength *HST* photometry from Piotto et al. (2015) is available for six AGB stars, while the remaining eleven stars have been identified only on

the CMD obtained from ground-based photometry.

2.2. The spectroscopic dataset

Our dataset consists of FLAMES-UVES spectra (RED580 setting, Pasquini et al. 2000) collected under the programs 093.D-0789 and 094.D-0455. Final spectra have been obtained by co-adding 2×2775 s and 30×2775 s exposures for M 4 and NGC 2808, respectively. Data were reduced using the UVES pipelines (Ballester et al. 2000), including bias subtraction, flat-field correction, wavelength calibration, sky subtraction and spectral rectification. The spectra have a spectral coverage of ~ 2000 Å with the central wavelength at ~ 5800 Å. Telluric subtraction has been performed by using the ESO MOLECFIT tool (Smette et al. 2015; Kaush et al. 2015). The typical signal to noise ratio for the final combined spectra around the [O I] $\lambda 6300$ Å line ranges from $S/N \sim 130$ to ~ 230 for M 4, and from ~ 160 to ~ 250 for NGC 2808.

Radial velocities (RVs) were derived using the `iraf@FXCOR` task, which cross-correlates the object spectrum with a template. For the template we used a synthetic spectrum obtained through MOOG (Sneden 1973), computed with a model stellar atmosphere interpolated from the Castelli & Kurucz (2004) grid, adopting parameters (effective temperature/surface gravity/microturbulence/metallicity) = (4900 K/2.0/2.0 km s⁻¹1.20). Each spectrum was corrected to the rest-frame system, and observed RVs were then corrected to the heliocentric system. The mean heliocentric RVs of M 4 and NGC 2808 are $\langle RV \rangle = +69.5 \pm 0.8$ km s⁻¹ ($\sigma = 3.2$ km s⁻¹) and $\langle RV \rangle = +96.7 \pm 3.9$ km s⁻¹ ($\sigma = 9.6$ km s⁻¹), respectively. These values agree with those obtained from RGB stars in the same clusters, e.g. $\langle RV \rangle = +70.6 \pm 1$ km s⁻¹ for M 4 (Marino et al. 2008), and $\langle RV \rangle = +102.4 \pm 1$ km s⁻¹ for NGC 2808 ($\sigma = 9.8$ km s⁻¹, Carretta et al. 2006). As discussed in Sect. 2.1, our spectroscopic targets had already passed the membership selection criterion based on proper motions. In the end, all proper-motion members are also RV members, with the exception of M4 star 16235035-2632478 (Table 1). Based on the chemical abundances, discussed in the next sections, the membership is further confirmed by the fact that all the target stars have [Fe/H] consistent with the cluster mean metallicity, except 1623035-2632478 which was not analyzed.

3. Chemical abundance analysis

Chemical abundances have been derived from a local thermodynamical equilibrium (LTE) analysis using MOOG (version 2013; Sneden 1973), plus α -enhanced model atmo-

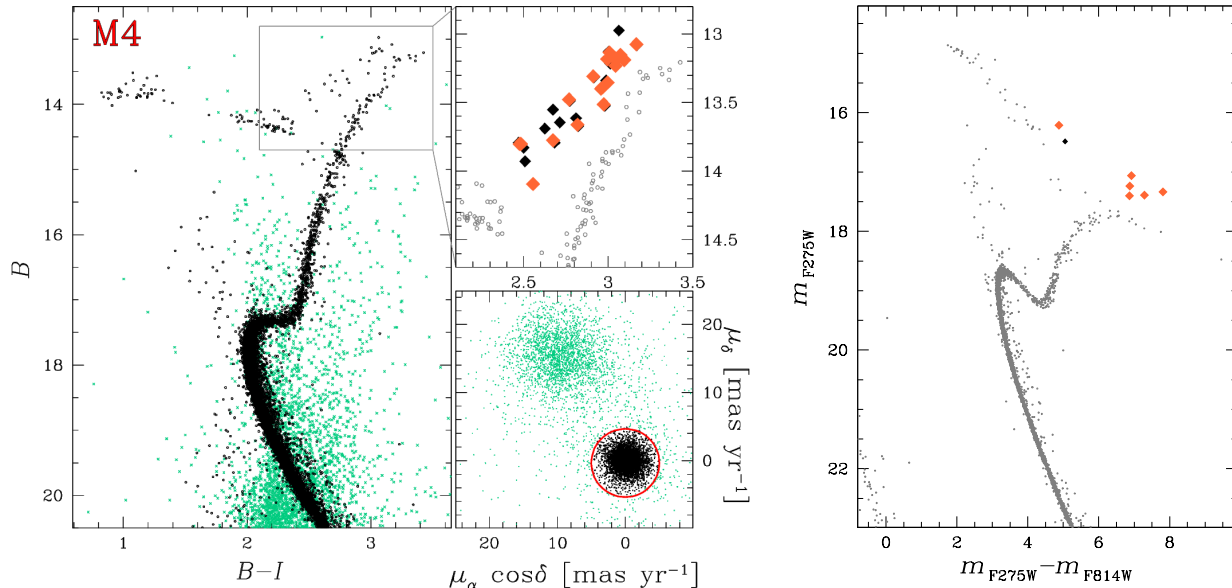


Fig. 1.— *Left panels:* B vs. $B - I$ CMD of stars with radial distance less than 20 arcmin from the center of M4 (Stetson et al. 2014). Cluster members and field stars are colored black and aqua, respectively, and have been selected on the basis of their proper motions. The vector-point diagram of stellar proper motions obtained by combining information from Gaia catalogues and WFI images is plotted on the lower-right side of the CMD. We also show a zoom of the CMD of cluster members around the AGB and the RGB. *Right panel:* m_{F275W} vs. $m_{F275W} - m_{F814W}$ CMD of NGC 2808 cluster members from HST photometry (Piotto et al. 2015). These AGB stars in the central HST field are also included in the ground-based photometry. The photometrically-selected AGB stars are indicated with filled diamonds in both CMDs, and those observed also spectroscopically are colored orange.

spheres of Castelli & Kurucz (2004). The line list and reference solar abundances are as in Marino et al. (2008).

To infer the atmospheric parameters used in our chemical analysis, we took advantage of the high-resolution and high-S/N of our UVES spectra and employed Fe lines. Specifically: (i) effective temperatures (T_{eff}) were derived by imposing the excitation potential equilibrium of the Fe I lines; (ii) surface gravities ($\log g$) were set with the ionisation equilibrium between Fe I and Fe II lines, but allowing Fe II abundances to be slightly higher than Fe I to take into account deviations from LTE (Lind et al. 2012; Bergemann et al. 2012); (iii) microturbulent velocities (ξ_t) were set to minimize any dependence on Fe I abundances on equivalent widths (EWs).

In Table 1 we list our adopted spectroscopic parameters, together with T_{eff} obtained

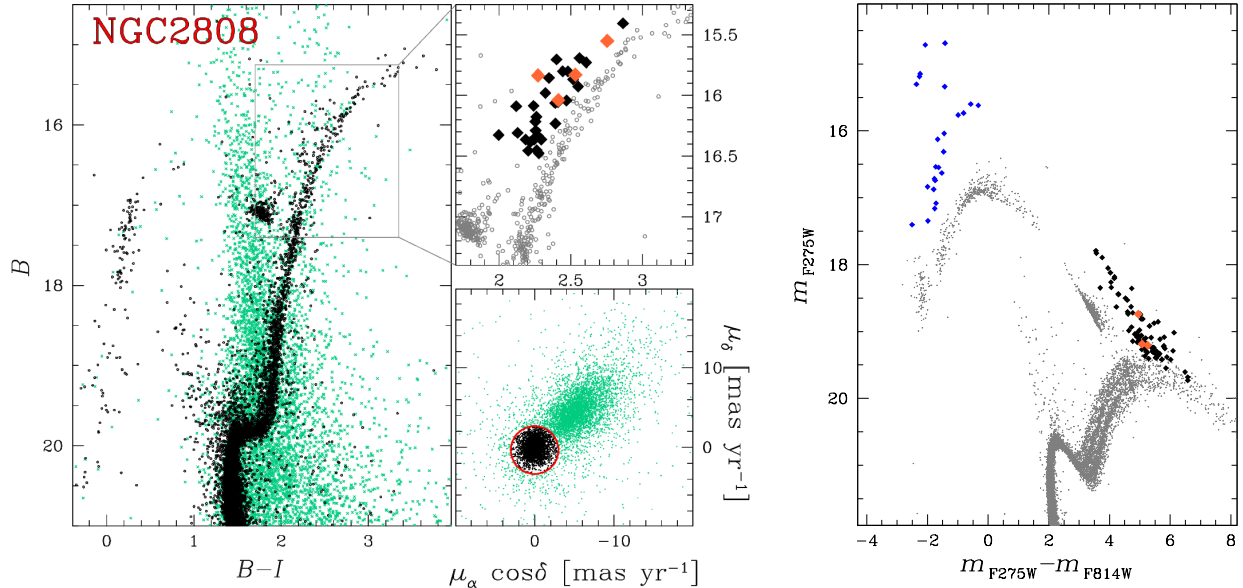


Fig. 2.— As in Figure 1 but for NGC 2808. In this case the CMD from ground-based photometry includes only stars with radial distance between 1.5 and 12.0 arcmin from the cluster center, and does not include the AGB observed in the central *HST* field. The blue points plotted in the right-panel CMD of cluster members mark candidate AGB-manqué stars.

from the Alonso ($B - V$)- T_{eff} calibrations (Alonso et al. 1999), assuming a reddening of $E(B - V)=0.36$ (Harris 1996) and $E(B - V)=0.19$ (Bedin et al. 2000) for M 4 and NGC 2808, respectively, and $\log g$ derived from the canonical relation assumed mass equal to $0.60 M_{\odot}$, $(m - M)_V=12.82$ for M 4, and $(m - M)_V=15.59$ for NGC 2808, temperatures, and apparent V magnitudes as above. By comparing the spectroscopically-derived atmospheric parameters with those from photometry we get mean differences of $\langle T_{\text{eff}B-V} - T_{\text{eff}Fe} \rangle = -12 \pm 15$ K, $\text{rms}=72$ K, and $\langle \log g_{\text{phot}} - \log g_{\text{Fe}} \rangle = -0.09 \pm 0.04$, $\text{rms}=0.21$. The fact that our adopted T_{eff} and $\log g$ average values agree reasonably with the photometric ones based on recent reddening values gives us confidence in our adopted T_{eff} scales. On the other hand, we notice that for M 4 AGBs, the discrepancy with the photometric temperatures is larger for hotter stars; specifically for stars with $T_{\text{eff}} > 4800$ K, the photometric temperatures and gravities are lower by >100 K and >0.2 , respectively². A variation in temperature of ± 100 K will change photometric surface gravities by around ± 0.05 - 0.06 dex only. Hence the discrepancy in T_{eff} alone is not enough to account for the lower photometric gravity in the higher-temperature

²The star with the highest discrepancy (star 16234268-2631209) has also a spectrum with broader lines, compared to the other stars, and, for this reason, we suggest caution with interpretation of this star.

stars. By changing the assumed mass by $\pm 0.1 M/M_{\odot}$, $\log g$ varies by around ± 0.08 dex. We are not able to explain why hotter stars display larger discrepancy between spectroscopic and photometric parameters in M4, which is not observed in NGC 2808, but note that in the latter case the observed range in T_{eff} is smaller ($\Delta T_{\text{eff}}=460$ K vs. $\Delta T_{\text{eff}}=790$ K in M4).

To test the magnitude of non-LTE effects on our metallicity values, assumed to be equal to Fe I abundances, we derived the non-LTE corrections to the Fe I spectral lines from Lind et al. (2012) by using the inspect tool³ for one RGB (#20766) and one AGB (#16233142-2633110) star in M4. We found that both the RGB and the AGB stars have positive non-LTE correction, 0.06 and 0.08 dex respectively. Hence, metallicities in non-LTE should be ~ 0.08 dex higher in our AGB sample. Note that the AGB non-LTE correction is only marginally higher (by 0.021 ± 0.002) than that of the RGB.

For all the elements, but O and Al, chemical abundances were obtained from the equivalent widths derived from Gaussian fitting of isolated spectral lines. Oxygen and aluminum were derived from spectral synthesis of the lines [O I] $\lambda 6300 \text{ \AA}$ and $\lambda 6363 \text{ \AA}$ and Al doublet $\lambda 6697 \text{ \AA}$ to account for the blending with other spectral features. In the end, we have been able to infer chemical abundances for sixteen elements, namely O, Na, Mg, Al, Si, Ca, Sc (Sc I and Sc II), Ti (Ti I and Ti II), V, Cr (Cr I and Cr II), Fe (Fe I and Fe II), Co, Ni, Zn, Y II and Ce II.

Estimates of the uncertainties in chemical abundances have been obtained by re-running the abundances varying $T_{\text{eff}}/\log g/[m/H]/\xi_t$, one at a time, by ± 100 K/ ± 0.20 / ± 0.15 / ± 0.30 km s⁻¹. The uncertainties used in T_{eff} and $\log g$ are reasonable as suggested by the comparison with the photometric values discussed above. As internal errors in $[m/H]$ and ξ_t we conservatively adopt ± 0.15 dex and ± 0.30 km s⁻¹. In addition to the contribution introduced by internal errors in atmospheric parameters, we estimated the contribution (σ_{fit}) due to the finite S/N, which affects the measurements of EWs and the spectral synthesis. The contribution due to EWs has been calculated by varying the EWs of spectral lines by $\pm 4.5 \text{ m\AA}$. This value has been derived by comparing EWs from various exposures of the same stars. The variations in the abundances obtained by varying the EWs have been then divided by $\sqrt{(N-1)}$ (where N is the number of available spectral lines). For the elements analysed through spectral synthesis we estimated the error in their chemical abundances by varying the continuum placement in the synthesis within a reasonable range. Variations in chemical abundances due to each contribution, plus the total error estimate obtained by summing in quadrature all the different contributions are listed in Tab. 2.

The average abundances and the corresponding uncertainties, defined as the rms from

³<http://inspect.coolstars19.com/index.php?n=Main.HomePage>

different spectral lines for the same species, are listed in Tables 3–5.

4. The chemical composition of multiple populations along the AGB

An illustration of our derived chemical abundances for AGB stars in M 4 and NGC 2808 is plotted in Fig. 3. The most obvious difference we observe among the AGBs of the two GCs is a much higher range in Al for NGC 2808. M 4 AGBs exhibit higher mean abundances for O, Mg, Si, Zn, and the neutron-capture elements Y and Ce. In analogy to what is observed among RGB stars, significant scatter is observed in both clusters for the elements involved in the high-temperature H-burning, namely O, Na; Al and Mg in the case of NGC 2808. This fact demonstrates that the AGBs of both M 4 and NGC 2808 host multiple stellar populations. Direct evidence of AGB stars with different Na and O abundances in M 4 is further provided in Fig. 4, where we compare the spectra of two stars with similar atmospheric parameters but different $[O/Fe]$ and $[Na/Fe]$. We note that the $[Fe/H]$ values are all consistent with cluster membership. The higher spreads in the Zn, Y II and Ce II abundances are most likely just the result of the small number of lines and larger errors. Indeed, the error estimates for these elements listed in Table 2 are relatively high, though we cannot exclude that they are over-estimated as they are higher than our observed rms values.

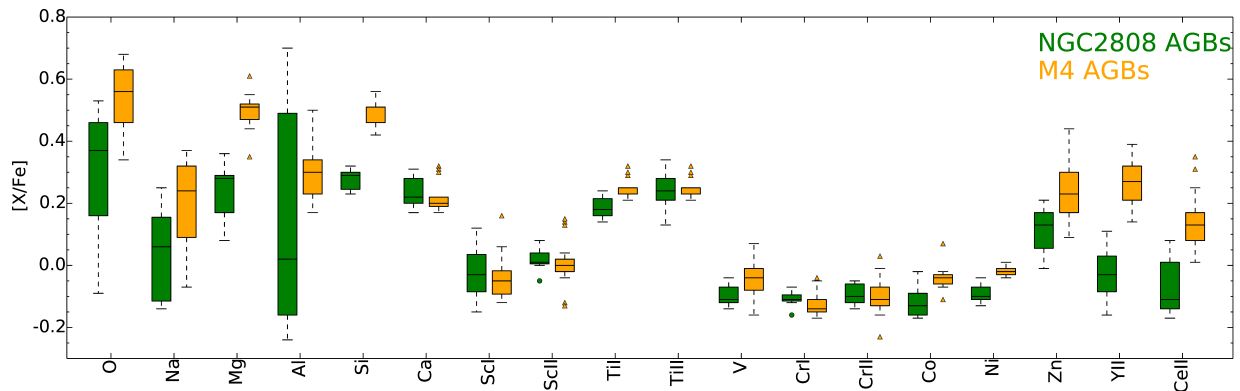


Fig. 3.— Box-and-whisker plot for the elemental abundances of AGB stars in NGC 2808 (green) and M 4 (orange). Each box represents the inner quartile of the distribution, and the median abundance is marked by the horizontal line. The whiskers include the 99.3% of the data, outliers are plotted by triangles.

A visual comparison between AGB and RGB abundances in the two analysed clusters is shown in Fig. 5. This comparison reveals that AGB and RGB exhibit similar distribution for most elements. The comparison does not extend beyond Ni because Zn, Y II and

Ce II abundances are not available for the RGB stars studied in Marino et al. (2008) and Carretta (2014, 2015).

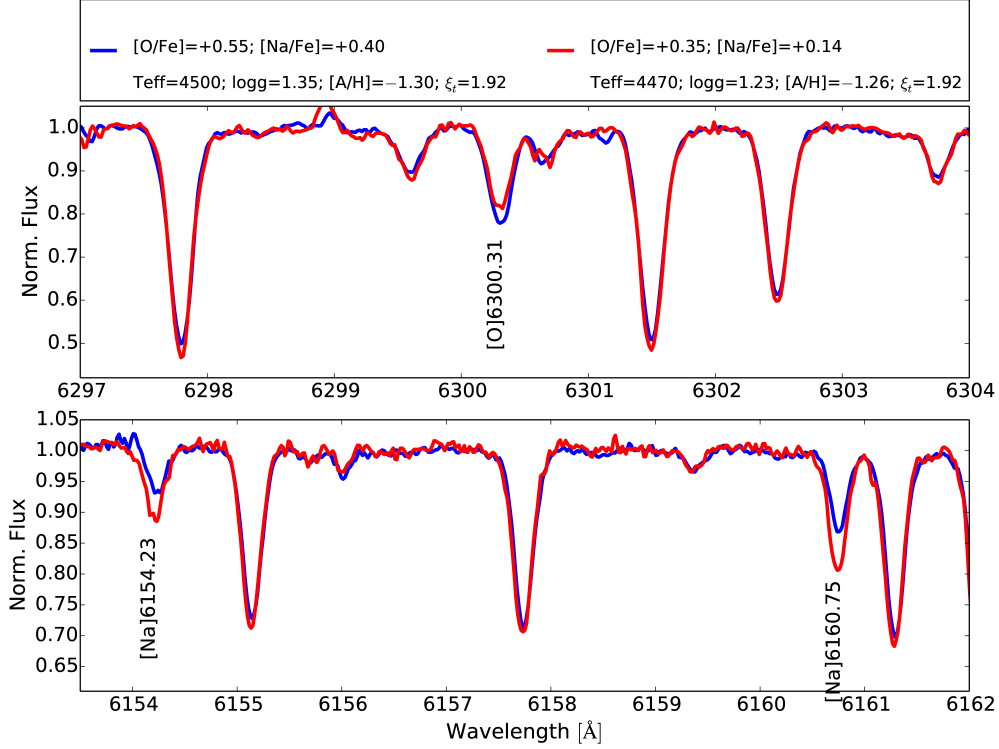


Fig. 4.— Comparison between the spectra of the AGB stars 16234740-2631463 (blue) and 16233667-2630397 (red), in M4. These stars have similar atmospheric parameters but different sodium and oxygen abundance.

Remarkable exceptions are the distributions of oxygen, sodium, magnesium and aluminum for NGC 2808, for which we observe differences in range between RGB and AGB stars. To properly compare these variations, we have calculated the difference, δ , between the 90th and the 10th percentile of the distribution of these elements for both RGB and AGB stars. We have also associated to each measurement an uncertainty that has been calculated by means of bootstrapping as in Milone et al. (2014) and which is indicative of the robustness of the δ determinations. For NGC 2808 a large and significant difference between the δ values for RGB and AGB stars has been derived for oxygen, ($\delta_{\text{RGB}}^{[\text{O}/\text{Fe}]} = 0.94 \pm 0.03$, $\delta_{\text{AGB}}^{[\text{O}/\text{Fe}]} = 0.60 \pm 0.09$). For Na, Mg and Al the differences in δ values are also large, but the significance is lower ($\delta_{\text{RGB}}^{[\text{Na}/\text{Fe}]} = 0.58 \pm 0.05$, $\delta_{\text{AGB}}^{[\text{Na}/\text{Fe}]} = 0.40 \pm 0.16$), ($\delta_{\text{RGB}}^{[\text{Mg}/\text{Fe}]} = 0.46 \pm 0.18$, $\delta_{\text{AGB}}^{[\text{Mg}/\text{Fe}]} = 0.18 \pm 0.05$), and ($\delta_{\text{RGB}}^{[\text{Al}/\text{Fe}]} = 1.13 \pm 0.13$, $\delta_{\text{AGB}}^{[\text{Al}/\text{Fe}]} = 0.77 \pm 0.40$). Further, as is apparent from Fig. 5, the results indicate that in NGC 2808 stars with the largest abundance of Na and Al and the lowest O and Mg content are clearly absent in the analyzed sample of

AGB stars. This suggests that the stellar population with extreme chemical composition in NGC 2808 avoids the AGB phase.

In contrast, the distributions of sodium and oxygen for RGB and AGB stars in M 4 are quite similar, even though the mean Na for AGBs is a bit lower ⁴. For this GC, we find $\delta_{\text{RGB}}^{[\text{O}/\text{Fe}]} = 0.26 \pm 0.02$ and $\delta_{\text{AGB}}^{[\text{O}/\text{Fe}]} = 0.24 \pm 0.06$ for oxygen, and $\delta_{\text{RGB}}^{[\text{Na}/\text{Fe}]} = 0.43 \pm 0.02$, $\delta_{\text{AGB}}^{[\text{Na}/\text{Fe}]} = 0.37 \pm 0.07$ for sodium. Further, there is no indication for any abundance distribution differences between the RGB and AGB stars for the other elements measured; this is also the case for NGC 2808 except for the differences already mentioned.

In the next sub-sections we present results on the light-element (anti-)correlations, and on the connection between chemical abundances and photometric properties of AGBs in M 4 (Sect. 4.1) and NGC 2808 (Sect. 4.2) in the context of multiple stellar populations.

4.1. The AGB of M 4

The upper panels of Figure 6 compare the position in the $[\text{Na}/\text{Fe}]$ vs. $[\text{O}/\text{Fe}]$ and the $[\text{Mg}/\text{Fe}]$ vs. $[\text{Al}/\text{Fe}]$ plane of the AGB stars analyzed in this paper and the RGB stars from Marino et al. (2008). AGB stars of M 4 clearly exhibit the Na-O anticorrelation, similar with what has been observed along the RGB, and both the RGB and the AGB clearly show two groups of Na-poor/O-rich and Na-rich/O-poor stars, although the AGB stars could either not reach the highest Na abundances observed on the RGB or could be shifted to lower values. There is no evidence for a Mg-Al anticorrelation neither along the RGB, nor the AGB, but we note that Na-rich AGB and RGB are slightly more-Al rich than Na-poor stars. The fractions of Na-poor/O-rich RGB and AGB stars are the same within one sigma. Specifically, the $42 \pm 5\%$ of RGB stars (37 out 88 stars) and the $53 \pm 13\%$ of AGB (9 out 17 stars) are considered Na-poor.

In contrast to our results, MacLean et al. (2016) suggested that in their sample of M 4 AGB stars only first generation stars were present, and that as a result, the M 4 AGB lacks second generation O-depleted, Na-rich stars. There are 10 stars in common between our M 4 AGB-star sample and that of MacLean et al. (2016). For these stars we find that our Na

⁴Note that Marino et al. (2008) applied an average non-LTE correction of -0.02 dex from Gratton et al. (1999) to the Na abundances of RGB stars, which are smaller than more recent computations by Lind et al. (2011). Hence, to not introduce systematics in our RGB-AGB comparison we do not apply any non-LTE correction to our AGB abundances. We warn the reader that, by comparing the RGB Na abundances from Marino et al. (2008) with those derived here, an additional small difference by 0.02 dex could be present, making the mean Na relative to Fe of RGB stars $+0.29$, instead of $+0.27$ dex.

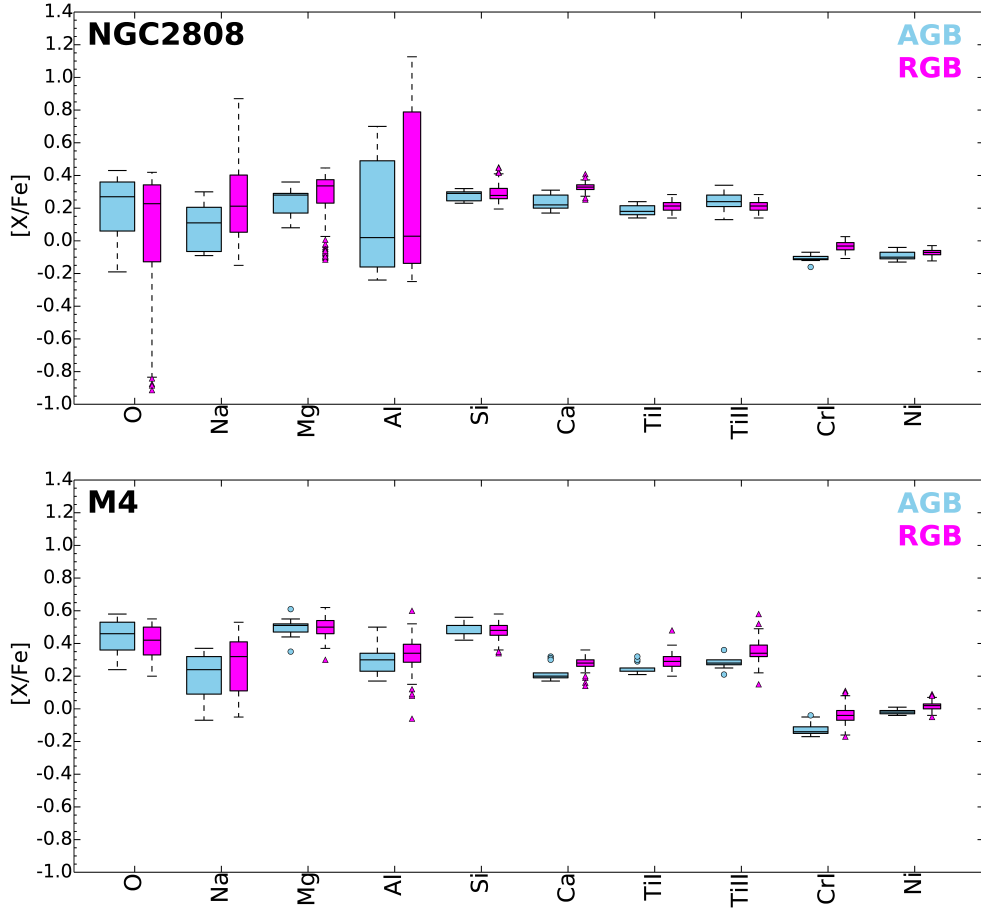


Fig. 5.— Box-and-whisker plot for the elemental abundance of AGB and RGB stars in NGC 2808 (upper panel) and M4 (lower panel), using the same vertical scale to emphasize the difference among the two clusters. The meaning of the boxes, whiskers and outliers is as in Fig. 3. Abundances for RGB stars of NGC 2808 and M4 are from Carretta (2014, 2015) and Marino et al. (2008), respectively. Due to the higher Al solar abundance used in this work, [Al/Fe] abundances for RGB stars both in M4 and NGC 2808 have been shifted by -0.21 dex.

abundances are 0.09 ± 0.01 dex (standard error of the mean) higher and our O abundances 0.06 ± 0.03 dex lower than the abundances listed in MacLean et al. (2016). These differences are consistent with the slightly different stellar parameters adopted: our temperatures are 65 K cooler (σ 55 K) and gravities 0.13 dex lower (σ 0.19 dex) than their values; and with different analysed spectral features: they use the 777 nm O triplet and the 568 nm Na doublet, while we use the forbidden O lines, and both the Na doublets at ~ 568 nm and ~ 616 nm. Intriguingly, if we plot the [Na/Fe] and [O/Fe] values from MacLean et al. (2016)

against each other solely for these 10 AGB stars, they clearly fall into two distinct groups, as do our abundances for the same stars (see Fig. 6, upper left panel), with one group having lower [O/Fe] and higher [Na/Fe] than the other. The same stars occupy each group in both samples, with one group have mean ([O/Fe], [Na/Fe]) of (0.55, -0.05) and the second having (0.45, 0.22), respectively, with the MacLean et al. (2016) abundances. This suggests the O-Na anti-correlation is indeed present in the MacLean et al. AGB star sample. The mean abundance differences between the two groups are essentially identical to that with our abundances: (Δ [O/Fe], Δ [Na/Fe]) is (-0.10 , $+0.27$) for the MacLean et al. abundances and (-0.17 , $+0.26$) for those presented here. We suggest that the conclusion of MacLean et al. (2016) that the M4 AGB lacks second generation stars may not be valid.

The apparent discrepancy with MacLean et al. might be reconciled by possible systematically lower Na in the AGB, than in the RGB counterpart. Our sample seems to suggest a systematic in the same direction, though much less pronounced. A similar phenomenon was already noticed by Ivans et al. (1999) for Na, and by Smith & Norris (1993) for the indices S(3839) (mostly sensitive to N) and W(G) (sensitive to C). Both studies report internal abundance dispersion on AGB, as on the RGB, but different abundances. Smith & Norris discussed possible causes for these discrepancies, including the C \rightarrow N processing occurring in the RGB envelopes which could make CN-strong red giants evolving to “less CN-enriched” AGBs. Furthermore, the same authors showed, through synthetic spectra computations, that the CN-band strengths on the AGB are less-pronounced than in the RGB due to different atmospheric parameters, causing the lower S3839 indices observed in AGB stars. This discussion probably enlightens that Na and O abundances might be better indicators of the primordial AGB abundances, although there could be some effects also on these elements. We suggest that star-to-star elemental internal variations are a much more reliable tool when we attempt a comparison between AGB and RGB stars in the context of multiple stellar populations.

To further compare the AGB with the RGB multiple populations pattern in M4, we take advantage of our photometry. It is well known that the two groups of RGB stars with different chemical compositions populate distinct sequences in the CMD or pseudo-CMD of M4 made with an appropriate combination of ultraviolet and optical filters (e.g. Marino et al. 2008; Monelli et al. 2013). In the lower-right panel of Figure 6 we reproduce the m_{F438W} vs. $C_{F275W,F336W,F438W}$ pseudo-CMD of M4 from Piotto et al. (2015), where the two main populations of M4 are clearly visible along the MS and the RGB. The two groups of Na-rich and Na-poor stars selected in the upper-left panel clearly correspond to the two main RGBs observed in this pseudo-CMD that we have obtained from *HST* photometry. We note that AGB stars span a much wider interval in $C_{F275W,F336W,F438W}$ than what we expect from observational errors only. Moreover, although *HST* photometry is available only for six stars

spectroscopically-analyzed in this paper, Na-rich AGB stars have smaller $C_{F275W,F336W,F438W}$ values than Na-poor AGB stars with the same luminosity in close analogy with what has been observed along the RGB.

The lower-left panel of Figure 6 plots the V vs. $C_{U,B,I}$ pseudo-CMD from ground-based photometry. This diagram has been recently used by Lardo et al. (2017) to show that both first- and second-generation stars climb the AGB of M4. Our diagram confirms that the $C_{U,B,I}$ spread for AGB is much larger than what we expect from photometric uncertainties only and is comparable to the $C_{U,B,I}$ spread of RGB stars with similar luminosity. As already shown by Monelli et al. (2013), the two populations of Na-rich and Na-poor RGB stars distribute along the two distinct RGB $C_{U,B,I}$ sequences of this cluster. The populations of Na-poor/O-rich and Na-rich/O-poor AGB stars exhibit a similar behaviour occupying different a location on the V vs. $C_{U,B,I}$ plane. These facts confirm that both the $C_{F275W,F336W,F438W}$ and the $C_{U,B,I}$ pseudo-colors are efficient to identify multiple stellar populations along the AGB of GCs and suggest that stars of both main populations of M4 climb the AGB.

4.2. The AGB of NGC 2808

Studies based on high-resolution spectroscopy of RGB stars have revealed that NGC 2808 exhibits very extended Na-O and Al-Mg anticorrelations as shown in the upper panels of Figure 7. Here the grey dots represent the $[Na/Fe]$ vs. $[O/Fe]$ and $[Al/Fe]$ vs. $[Mg/Fe]$ for RGB stars from Carretta (2014, 2015). Photometry has shown that the MS and RGB of NGC 2808 host at least five stellar populations, namely A–E, identified by means of the “chromosome map” tool able to maximise the separation between stellar populations with different chemical content. The “chromosome map” of NGC 2808 RGBs published in Milone et al. (2015a) is reproduced in the lower-right panel of Figure 8, with the different populations represented in different colors. Populations A–E have indeed distinct combinations of light-elements/helium abundances (Milone et al. 2015a): (i) Populations E and D have very high helium content ($Y \sim 0.38$ and $Y \sim 0.32$, respectively) and extreme abundances of N, O, Na, Mg, and Al. They are clearly separated from the remaining stars in both the $[Na/Fe]$ - $[O/Fe]$ and the $[Al/Fe]$ - $[Mg/Fe]$ plane and correspond to the groups of stars with $[O/Fe] < -0.2$ and $-0.2 < [Mg/Fe] < 0.2$ shown in Figure 7. (ii) Stellar populations B and C, which have low sodium and aluminum content, are not clearly distinguishable in the diagrams of Figure 7. (iii) There is no spectroscopic information on population-A stars, which, according to multi-wavelength photometry have similar light-element abundance as populations B and C.

In this Section we compare the chemical abundances and the photometry of AGB stars

with results on multiple RGBs from the literature and attempt to connect the populations along the AGB, the RGB, and the MS. In the upper panels of Fig. 7 we compare our Na-O and Al-Mg anticorrelations obtained from the AGB stars with those on the RGB. This comparison clearly reveals that, among the analyzed AGB stars, $[\text{Na}/\text{Fe}]$ anticorrelates with $[\text{O}/\text{Fe}]$ while $[\text{Al}/\text{Fe}]$ anticorrelates with $[\text{Mg}/\text{Fe}]$, qualitatively confirming that the AGB exhibits the same chemical pattern as the RGB. The obvious difference between AGBs and RGBs is that the AGBs do not reach extremely O-poor and Mg-poor abundances, as RGBs do.

Comparing with the chemical composition observed on the “chromosome map” by Milone et al. (2015a), the two AGBs with $[\text{O}/\text{Fe}] < 0.0$ have chemical composition consistent with population-D RGB stars and are represented with magenta starred symbols in Figure 7. Two out of the five AGB stars with $[\text{O}/\text{Fe}] > 0.0$ have slightly-higher sodium and aluminum abundance than the remaining AGB stars. They share the same chemical composition as population-C RGB stars and are represented with red triangles. The blue circles represent the remaining three stars with $[\text{Na}/\text{Fe}] < 0.0$, which have similar chemical abundance as population-B RGB stars. For simplicity, in the following, we will refer to the groups of stars colored blue, red, and magenta, as groups 1, 2, and 3.

The most extreme RGB stars in terms of chemical composition, e.g. those with the highest He and lowest O, are those belonging to population-E on the “chromosome map”. None of the seven analyzed AGB stars belong to this group. This fact can be either due to the small number of studied AGB stars or to the lack of stars with extreme chemical composition along the AGB. By assuming that the population E includes 15% of the total number of NGC 2808 stars (e.g. Simioni et al. 2016) the probability that the lack of AGB population-E stars is due to the small statistical sample, inferred from Monte-Carlo simulations, is 0.32. Therefore, without additional AGB stars spectroscopically analyzed we cannot draw a firm conclusion. By accounting for the radial distribution of different stellar populations, we know that population-E stars are more-centrally concentrated than the other stars of NGC 2808, and the fraction of population-E stars with respect to the total number of cluster stars ranges from $21 \pm 3\%$ for radial distance $R < 0.6$ arcmin to $9 \pm 5\%$ for $R > 5.5$ arcmin (Simioni et al. 2016). By assuming these extreme values for the fraction of population-E stars we find that the probability that the lack of AGB population-E stars is due to the small statistical sample is 17% and 50%, respectively. These numbers support the previous conclusion that due to the small number of analyzed stars, we cannot draw any strong conclusion about the lack of population-E stars along the AGB from spectroscopy only. Nevertheless, population-E RGB stars are likely to evolve to become the hottest HB stars which will then fail to reach the AGB. So, even if the statistics is poor, the evidence is consistent with the posit that population-E does not reach the AGB.

Hence, to further investigate multiple populations along the AGB of NGC 2808 we combine information from both spectroscopy and photometry. As shown in the lower-right panel of Figure 7, the AGB of NGC 2808 splits into three distinct sequences in the m_{F438W} vs. $C_{F275W,F336W,F438W}$ pseudo-CMD. We have analyzed the spectra of one star in each of the three sequences and find that the three stars belong to the three different groups 1, 2, and 3, as previously defined. Therefore they have distinct light-element content with the Na abundance increasing from the lowest to the highest value of $C_{F275W,F336W,F438W}$.

Similarly to the AGB, the RGB of NGC 2808 exhibits three main sequences in the m_{F438W} vs. $C_{F275W,F336W,F438W}$ pseudo-CMD (Piotto et al. 2015; Milone et al. 2015a). Most of the difference in the $C_{F275W,F336W,F438W}$ pseudo-color among stars with the same magnitude is interpreted as the effect of light-element variation in the spectrum of the star. Thus, we expect that stars in the three AGB photometric sequences, shown in the lower-right panel of Figure 7, are associated with the three corresponding main RGBs.

The fact that the AGB of NGC 2808 is not consistent with a simple population is further supported by the V vs. $C_{U,B,I}$ pseudo-CMD from ground-based photometry plotted in the lower-left panel of Figure 7, where the $C_{U,B,I}$ dispersion of AGB stars is significantly larger than that expected from observational errors only. In contrast with the RGB, where there is a clear correlation (anti-correlation) between the $C_{U,B,I}$ value of a star and its sodium (oxygen) abundance (Monelli et al. 2013), the small number of analyzed AGB stars prevents us from any strong conclusion about the possible correlation between the light-element abundance of an AGB star and its $C_{U,B,I}$ pseudo-color. Nevertheless, we note that Na-poor AGB stars have smaller $C_{U,B,I}$ values than Na-rich AGB stars, in close analogy with what we have observed in M 4.⁵

In the lower-left panel of Figure 8, we plotted the $\Delta_{CF275W,F336W,F438W}$ vs. $\Delta_{F275W,F814W}$ pseudo-CMD or ‘chromosome’ map of AGB stars in NGC 2808 that we have derived by extending to AGB stars the method that we have previously introduced for the RGB (Milone et al. 2015a). The lower-right panel of the same figure reproduces the same diagram derived for RGB stars and marks the main populations A–E of NGC 2808 with different colors. In

⁵We note that the two stellar populations of AGB and RGB stars in M 4 distribute along two distinct sequences in the V vs. $C_{U,B,I}$ diagram, in contrast with what we observe in NGC 2808 where it is impossible to distinguish the different stellar populations along the RGB and AGB by using the $C_{U,B,I}$ index only (see Monelli et al. 2013 for the $C_{U,B,I}$ distribution of RGB stars). The position of a star in the V vs. $C_{U,B,I}$ pseudo-CMD depends on its abundance of helium and light elements and accurate study involving isochrones and synthetic spectra with appropriate chemical composition is mandatory to fully understand the observed distribution of stars in the V vs. $C_{U,B,I}$ (see e.g. Dotter et al. 2015 for NGC 6752). Similar conclusion can be extended to the m_{F438W} vs. $C_{F275W,F336W,F438W}$ diagram.

contrast to the observations of MS and RGB stars, where at least five stellar populations are present in the chromosome map, the lower-left panel of Figure 8 reveals only three groups of AGB stars. For example, relative to the number of population D stars on the AGB, there are many fewer stars in the population E region. Similarly, there is an apparent dearth of AGB stars in the population A region.

We followed the recipe by McLachlan & Peel (2000) to derive the groups of AGB stars that are statistically significant. Briefly, we determined the maximum-likelihood fit to various numbers of groups and calculated the optimal number of groups by using the Bayesian information criterion (BIC) penalized likelihood measure for model complexity. To this aim, we did vary the size and the shape of the distinct groups of AGB stars. For each combination of shape and size, we assumed a number, N of populations from 1 to 8, and calculated a BIC value. The most likely explanation corresponds to $\text{BIC}=79.2$ and $N = 4$ with the assumption that the groups have equal shape and variable volume and orientations (VEV). Similarly, the second best BIC value ($\text{BIC}=74.2$) corresponds to $N = 4$ and stellar groups with variable shape, volume and orientations (VVV). The resulting three main groups of stars are colored in blue, red, magenta, in Fig. 8. The fourth stellar group includes six only outliers that have been colored black. The results support the visual impression that the AGB of NGC 2808 hosts only three main stellar, strengthening the idea that stars with extreme He and O do not evolve through the AGB phase.

We note that the “chromosome maps” of RGB and AGB stars reveal significant differences. Specifically, only one group of stars with $\Delta_{\text{F275W,F336W,F438W}} \sim 0.0$ is present along the AGB, in contrast with what we observe along the RGB where we clearly distinguish the two groups of population-A and population-B stars. It remains unclear whether population-A stars do not exist along the AGB or if they are mixed with population-B.

Moreover, while we clearly observe population-D and -E stars along the RGB and the MS, only one group of AGB stars with large values $\Delta_{\text{F275W,F336W,F438W}}$ is present. To investigate the presence of population-E AGB stars in the upper panels of Figure 8 we compare the $\Delta_{\text{F275W,F814W}}$ histogram distribution of AGB stars and RGB stars. As discussed in Milone et al. (2015a, see their Fig. 3) the RGB of NGC 2808 is consistent with three main peaks that correspond to population E, D, and to the group of populations A+B+C. In contrast, along the AGB we distinguish a dominant peak, associated to the stellar groups 1 and 2, plus a stellar tail mostly due to group-3 stars.

If group-3 includes both populations D and E the fraction of group-3 stars with respect to the total number of AGB stars should be consistent with the ratio between population D+E RGB stars and the total number of RGB stars. We find that group 3 includes $27 \pm 5\%$ of the total number of AGB. This value significantly differs from the ratio of RGB-D+E

stars with respect to the total number of AGB stars that is $50\pm 1\%$. In contrast, the ratio between RGB-D stars and the number of RGB-A+B+C+D star is $30\pm 1\%$ and is consistent within one sigma with the fraction of group-3 AGB stars with respect to the total number of AGB stars. These results are consistent with the lack of population-E stars along the AGB.

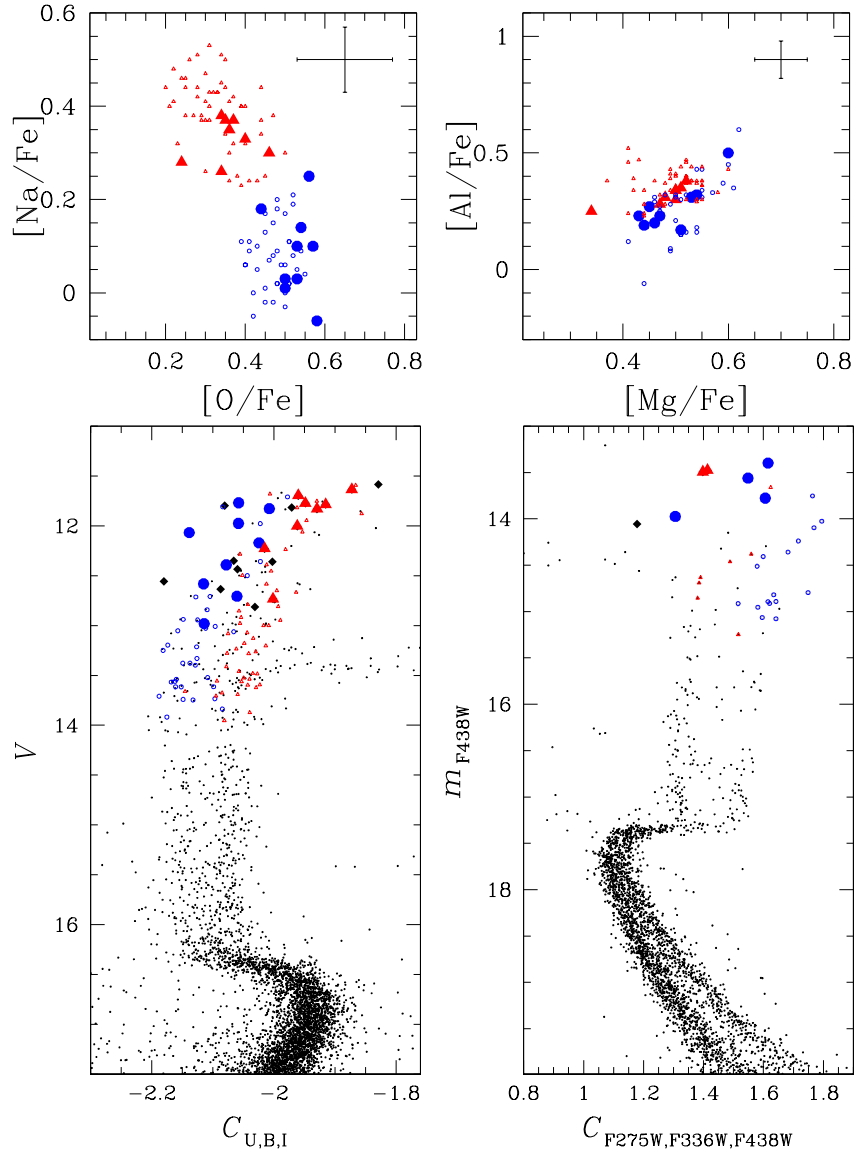


Fig. 6.— *Upper panels:* Sodium vs. oxygen (left), aluminum vs. magnesium (right) for AGB stars in M4. The lower panels show the V vs. $C_{U,B,I}$ (left) and m_{F438W} vs. $C_{F275W,F336W,F438W}$ (right) pseudo-CMDs for M4 stars. AGB and RGB stars analyzed spectroscopically in this paper and in Marino et al. (2008) are represented with large and small symbols, respectively. The two populations of Na-poor/O-rich and Na-rich/O-poor RGB and AGB stars are shown as blue filled circles and red filled triangles, respectively, while the remaining AGB stars that have been not analyzed spectroscopically are represented with black diamonds in the lower-panel diagrams. To put Al abundances on the same scale for AGBs and RGBs, we subtract 0.21 to the RGB abundances (see Fig. 5).

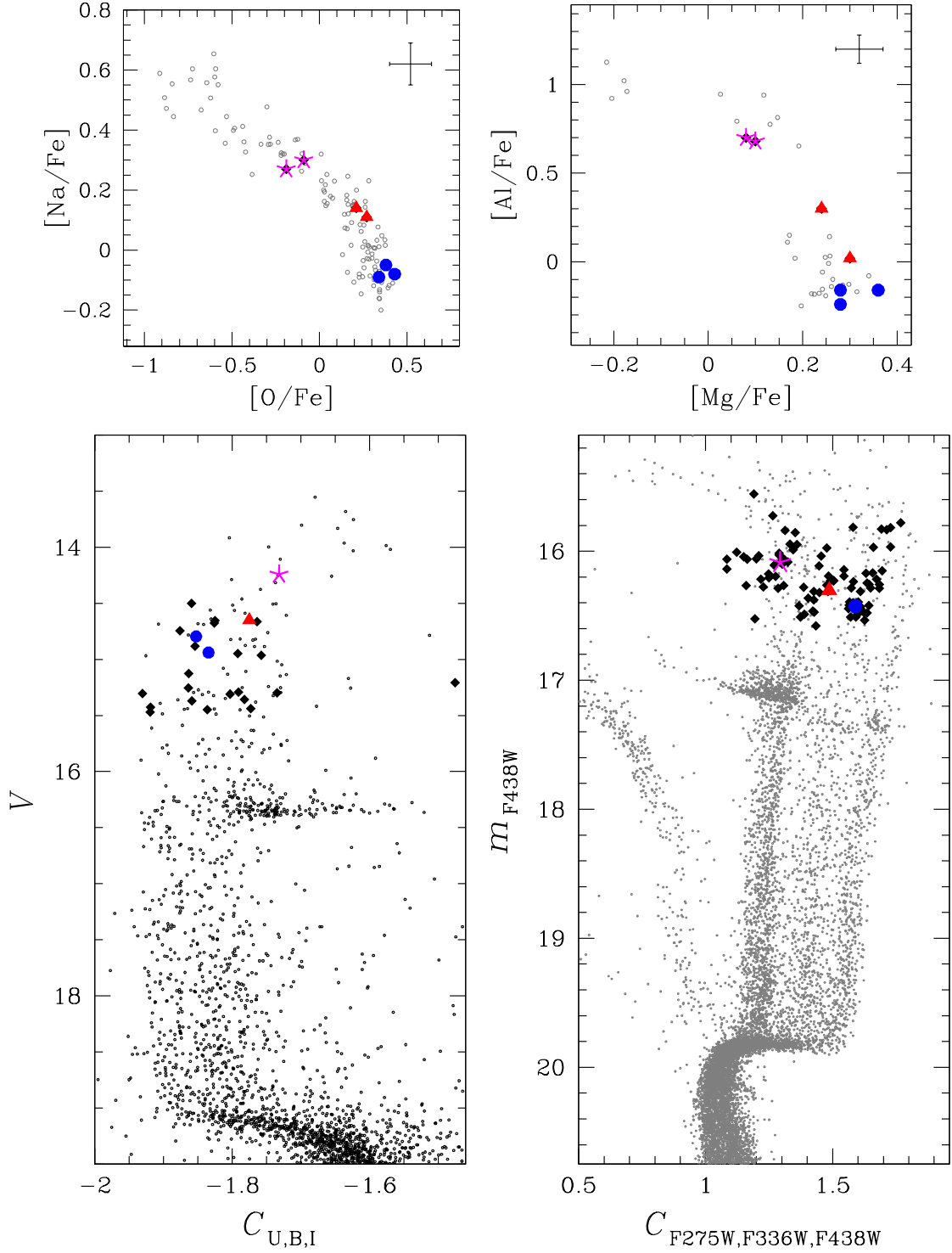


Fig. 7.— *Upper panels:* Sodium-oxygen and magnesium-aluminum anticorrelation for RGB stars (grey circles, Carretta 2014, 2015) and AGB stars (colored symbols). *Lower panels:* V vs. $C_{U,B,I}$ (left) and m_{F438W} vs. $C_{F275W,F336W,F438W}$ (right) pseudo-CMDs of NGC 2808 stars. AGB stars are indicated with black diamonds, while the groups 1, 2, and 3 of AGB stars (observed spectroscopically), selected on the basis of their position in the $[\text{Na}/\text{Fe}]$ vs. $[\text{O}/\text{Fe}]$ plane, are represented with blue dots, red triangles, and magenta starred symbols, respectively. As for Figs. 5 and 6, Al abundances of RGB stars have been decreased by 0.21 dex,

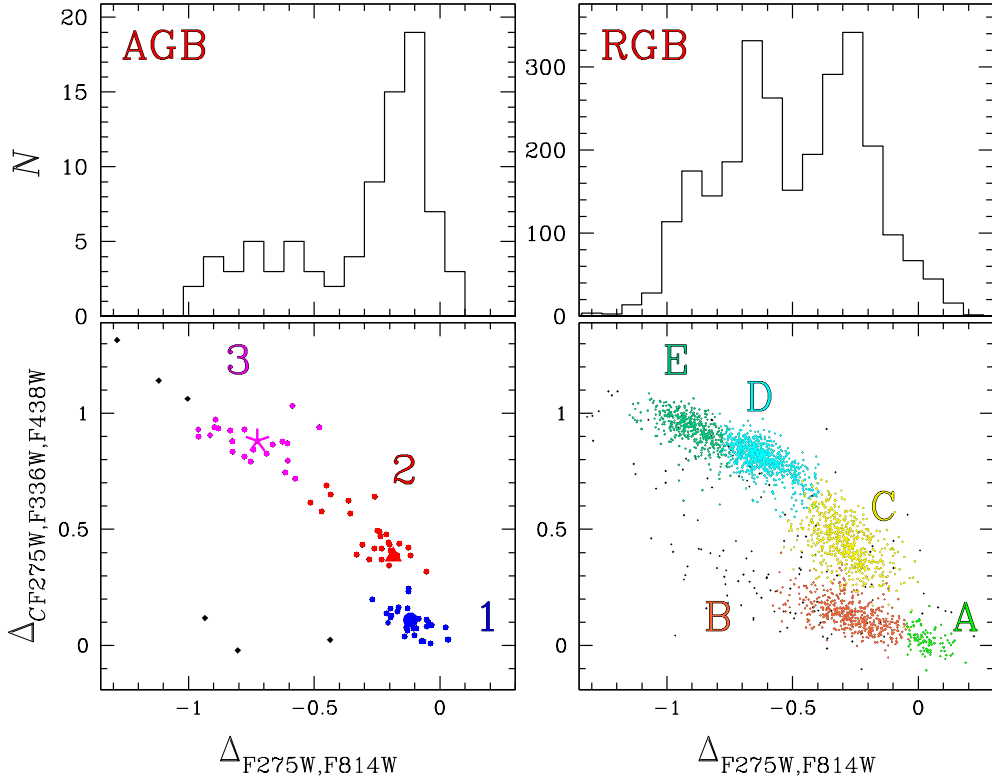


Fig. 8.— *Upper panels:* $\Delta_{F275W,F814W}$ histogram distribution for AGB (left) and RGB stars (right) in NGC 2808. *Lower panels:* $\Delta_{CF275W,F336W,F438W}$ vs. $\Delta_{F275W,F814W}$ pseudo two-color diagram, or ‘chromosome map’ of AGB (left) and RGB stars (right) in NGC 2808 from Milone et al. (2015a). The groups 1, 2, and 3 of AGB stars are colored blue, red, and magenta, respectively, while large colored symbols indicate our spectroscopic AGB targets. The five populations, A–E, of RGB stars are colored green, orange, yellow, cyan, and aqua, respectively. Outliers not assigned to any population are represented as black points in both the AGB and RGB chromosome map.

ID (2MASS)	GC	RA J2000	DEC J2000	RV [km s ⁻¹]	T _{eff} [K]	log <i>g</i> [cgs]	[Fe/H]	ξ _t [km s ⁻¹]	T _{eff} (phot) [K]	log <i>g</i> (phot) [cgs]
16233067-2629390	M 4	16:23:30.70	-26:29:39.0	+72.88	4920	1.85	-1.18	1.81	4817	1.77
16233741-2638238	M 4	16:23:37.44	-26:38:23.9	+66.88	4770	1.50	-1.22	1.72	4732	1.58
16234268-2631209	M 4	16:23:42.71	-26:31:20.8	+74.01	5190	2.25	-1.07	1.78	5022	1.92
16233020-2633241	M 4	16:23:30.23	-26:33:24.0	+67.26	4630	1.55	-1.19	1.91	4641	1.44
16235035-2632478	M 4	16:23:50.38	-26:32:47.8	-48.01	-	-	-	-	-	-
16233142-2633110	M 4	16:23:31.45	-26:33:10.9	+65.80	4400	1.25	-1.18	2.00	4445	1.18
16233846-2629235	M 4	16:23:38.49	-26:29:23.5	+68.32	4780	1.75	-1.17	1.82	4701	1.63
16233535-2632225	M 4	16:23:35.37	-26:32:22.5	+67.83	4450	1.20	-1.26	1.92	4497	1.27
16240858-2624552	M 4	16:24:08.60	-26:24:55.2	+72.82	4680	1.60	-1.27	1.82	4623	1.46
16233477-2631349	M 4	16:23:34.79	-26:31:34.9	+69.68	5150	2.50	-1.22	1.62	5023	1.92
16234740-2631463	M 4	16:23:47.41	-26:31:46.3	+72.98	4500	1.35	-1.28	1.92	4536	1.32
16232988-2631490	M 4	16:23:29.90	-26:31:49.0	+71.86	4530	1.40	-1.28	1.77	4561	1.39
16235375-2634426	M 4	16:23:53.77	-26:34:42.6	+65.54	4530	1.40	-1.21	1.93	4547	1.31
16233667-2630397	M 4	16:23:36.69	-26:30:39.7	+63.13	4470	1.23	-1.24	1.92	4508	1.28
16233614-2632015	M 4	16:23:36.17	-26:32:01.5	+67.30	4570	1.75	-1.12	1.57	4570	1.31
16231672-2634279	M 4	16:23:16.75	-26:34:28.0	+72.19	4500	1.40	-1.24	1.96	4435	1.20
16234085-2631215	M 4	16:23:40.88	-26:31:21.5	+71.45	4550	1.60	-1.18	1.70	4587	1.48
16232114-2631598	M 4	16:23:21.17	-26:31:59.7	+71.96	5090	2.47	-1.14	1.61	4964	2.00
09120251-6451001	NGC 2808	09:12:02.51	-64:51:00.2	+96.61	4750	1.55	-1.31	1.70	4773	1.66
09123016-6454129	NGC 2808	09:12:30.18	-64:54:12.9	+99.14	4770	1.78	-1.20	1.55	4796	1.54
09120852-6449107	NGC 2808	09:12:08.53	-64:49:10.7	+110.92	4630	1.55	-1.19	1.75	4690	1.55
09120213-6452243	NGC 2808	09:12:02.15	-64:52:24.4	+87.84	4860	1.55	-1.30	1.82	4788	1.62
09122027-6448450	NGC 2808	09:12:20.29	-64:48:45.1	+86.07	4500	1.15	-1.32	1.75	4579	1.36
09120665-6450253	NGC 2808	09:12:06.66	-64:50:25.4	+106.72	4800	1.60	-1.30	1.70	4887	1.80
09114655-6452144	NGC 2808	09:11:46.55	-64:52:14.5	+89.63	4400	0.90	-1.25	2.05	4420	1.07

Table 1: Coordinates, radial velocities, and atmospheric parameters of the AGB stars spectroscopically analysed in this paper.

Table 2: Sensitivity of derived abundances to the uncertainties in atmospheric parameters, the limited S/N (σ_{fit}) and the total error due to these contributions (σ_{tot}).

	ΔT_{eff}	$\Delta \log g$	$\Delta \xi_t$	$\Delta [m/H]$	σ_{fit}	σ_{total}
	$\pm 100 \text{ K}$	± 0.20	$\pm 0.30 \text{ km s}^{-1}$	0.15 dex		
[O/Fe]	± 0.02	± 0.09	∓ 0.01	∓ 0.05	± 0.06	0.12
[Na/Fe]	∓ 0.02	∓ 0.01	± 0.03	∓ 0.01	± 0.06	0.07
[Mg/Fe]	∓ 0.03	∓ 0.01	± 0.00	∓ 0.00	± 0.04	0.05
[Al/Fe]	± 0.07	∓ 0.00	∓ 0.00	± 0.01	± 0.04	0.08
[Si/Fe]	∓ 0.08	± 0.02	± 0.04	± 0.02	± 0.07	0.12
[Ca/Fe]	± 0.01	∓ 0.02	∓ 0.04	∓ 0.01	± 0.01	0.05
[Sc/Fe] I	± 0.00	± 0.01	± 0.04	± 0.01	± 0.03	0.05
[Sc/Fe] II	± 0.05	∓ 0.01	∓ 0.03	± 0.01	± 0.05	0.08
[Ti/Fe] I	± 0.06	∓ 0.01	∓ 0.01	∓ 0.01	± 0.01	0.06
[Ti/Fe] II	± 0.04	∓ 0.01	∓ 0.06	∓ 0.01	± 0.03	0.08
[V/Fe]	± 0.07	∓ 0.01	± 0.02	∓ 0.01	± 0.03	0.08
[Cr/Fe] I	± 0.04	∓ 0.01	∓ 0.02	∓ 0.01	± 0.02	0.05
[Cr/Fe] II	± 0.01	∓ 0.01	± 0.02	∓ 0.01	± 0.04	0.05
[Fe/H] I	± 0.10	± 0.01	∓ 0.06	± 0.00	± 0.01	0.12
[Fe/H] II	∓ 0.06	± 0.09	∓ 0.03	± 0.04	± 0.04	0.13
[Co/Fe]	∓ 0.01	± 0.00	± 0.05	± 0.01	± 0.04	0.07
[Ni/Fe]	∓ 0.02	± 0.01	± 0.03	± 0.01	± 0.01	0.04
[Zn/Fe]	∓ 0.13	± 0.04	∓ 0.07	± 0.02	± 0.02	0.16
[Y/Fe] II	± 0.06	∓ 0.01	∓ 0.09	∓ 0.00	± 0.05	0.12
[Ce/Fe] II	± 0.08	∓ 0.01	± 0.01	± 0.01	± 0.07	0.11

Table 3: Derived chemical abundances for O, Na, Mg, Al, Si, and Ca in M 4 and NGC 2808 AGBs.

ID (2MASS)	[O/Fe]	rms/#	[Na/Fe]	rms/#	[Mg/Fe]	rms/#	[Al/Fe]	rms/#	[Si/Fe]	rms/#	[Ca/Fe]	rms/#
M 4												
16233142-2633110	+0.34	0.04/2	+0.25	0.13/3	+0.51	0.07/3	+0.34	0.04/2	+0.49	0.01/3	+0.19	0.09/13
16233477-2631349	+0.57	0.02/2	+0.09	0.12/3	+0.46	0.09/2	+0.27	0.06/2	+0.42	0.04/3	+0.32	0.09/14
16233535-2632225	+0.34	0.04/2	+0.37	0.09/3	+0.53	0.00/2	+0.38	0.03/2	+0.51	0.04/3	+0.20	0.08/13
16233614-2632015	+0.56	0.02/2	+0.24	0.07/3	+0.44	0.02/3	+0.23	0.00/2	+0.42	0.06/3	+0.31	0.09/13
16233741-2638238	+0.24	0.04/2	+0.27	0.14/3	+0.48	0.09/2	+0.28	0.02/2	+0.46	0.01/3	+0.21	0.11/12
16234085-2631215	+0.53	0.01/2	+0.02	0.06/3	+0.61	0.00/2	+0.50	0.05/2	+0.56	0.02/3	+0.21	0.10/13
16234268-2631209	+0.40	0.01/2	+0.32	0.16/4	+0.35	- /1	+0.25	0.04/2	+0.47	0.02/3	+0.30	0.10/11
16234740-2631463	+0.53	0.03/2	+0.09	0.06/3	+0.54	0.02/3	+0.31	0.02/2	+0.51	0.04/3	+0.18	0.09/13
16235375-2634426	+0.37	0.04/2	+0.36	0.08/3	+0.49	0.04/3	+0.31	0.03/2	+0.53	0.06/2	+0.18	0.10/13
16240858-2624552	+0.58	0.02/2	-0.07	0.10/3	+0.47	0.06/2	+0.20	0.04/2	+0.45	0.07/3	+0.17	0.09/13
16231672-2634279	+0.46	0.01/2	+0.29	0.06/3	+0.51	0.02/2	+0.30	0.01/2	+0.51	0.05/3	+0.17	0.10/13
16232114-2631598	+0.54	0.13/2	+0.13	0.07/4	+0.45	0.06/2	+0.19	0.04/2	+0.46	0.07/3	+0.30	0.08/13
16232988-2631490	+0.50	0.01/2	+0.02	0.08/3	+0.55	0.01/2	+0.32	0.04/2	+0.51	0.03/3	+0.19	0.09/13
16233020-2633241	+0.35	0.04/2	+0.36	0.19/4	+0.51	0.05/2	+0.34	0.04/2	+0.52	0.03/3	+0.20	0.10/12
16233067-2629390	+0.50	0.06/2	+0.00	0.13/4	+0.52	0.22/2	+0.17	0.01/2	+0.52	0.02/2	+0.22	0.11/ 9
16233667-2630397	+0.36	0.01/2	+0.34	0.06/3	+0.52	0.01/3	+0.35	0.01/2	+0.51	0.04/3	+0.19	0.09/12
16233846-2629235	+0.44	0.04/2	+0.17	0.09/3	+0.48	0.06/2	+0.23	0.01/2	+0.46	0.05/3	+0.20	0.09/12
mean	+0.45		+0.19		+0.50		+0.29		+0.49		+0.22	
±	0.02		0.04		0.01		0.02		0.01		0.01	
rms	0.10		0.14		0.05		0.08		0.04		0.04	
NGC 2808												
09120665-6450253	+0.38	0.03/2	-0.05	0.07/4	+0.28	0.01/2	-0.16	0.00/2	+0.32	0.09/3	+0.26	0.09/14
09120251-6451001	+0.27	0.07/2	+0.11	0.11/4	+0.24	0.04/2	+0.30	0.04/2	+0.23	0.02/3	+0.22	0.10/11
09120213-6452243	-0.19	0.09/2	+0.27	0.07/4	+0.08	0.14/2	+0.70	0.01/2	+0.30	0.03/3	+0.17	0.13/12
09114655-6452144	-0.09	0.08/2	+0.30	0.10/4	+0.10	0.02/3	+0.68	0.03/2	+0.29	0.05/3	+0.18	0.11/10
09122027-6448450	+0.21	0.01/2	+0.14	0.09/4	+0.30	0.05/3	+0.02	0.01/2	+0.25	0.06/3	+0.22	0.11/13
09123016-6454129	+0.34	0.04/2	-0.09	0.11/4	+0.28	0.01/3	-0.24	0.07/2	+0.24	0.04/3	+0.31	0.10/14
09120852-6449107	+0.43	0.04/2	-0.08	0.13/4	+0.36	0.06/2	-0.16	0.04/2	+0.30	0.14/2	+0.30	0.08/14
mean	+0.19		+0.09		+0.23		+0.16		+0.28		+0.24	
±	0.09		0.06		0.04		0.15		0.01		0.02	
rms	0.22		0.15		0.10		0.37		0.03		0.05	

Table 4: Derived chemical abundances for Sc, Ti, V, and Cr in M 4 and NGC 2808 AGBs.

ID (2MASS)	[Sc/Fe] I	rms/#	[Sc/Fe] II	rms/#	[Ti/Fe] I	rms/#	[Ti/Fe] II	rms/#	[V/Fe]	rms/#	[Cr/Fe] I	rms/#	[Cr/Fe] II	rms/#	
M 4															
16233142-2633110	-	- /0	+0.01	0.11/6	+0.22	0.06/15	+0.30	0.15/5	-0.12	0.30/13	-0.12	0.14/10	-0.05	0.04/2	
16233477-2631349	-0.02	- /1	+0.14	0.04/6	+0.32	0.08/15	+0.36	0.08/5	+0.01	0.11/10	-0.06	0.10/ 7	-0.01	0.02/2	
16233535-2632225	-0.07	- /1	-0.01	0.07/5	+0.23	0.05/16	+0.21	0.06/4	-0.03	0.08/12	-0.16	0.11/ 7	-0.08	- /1	
16233614-2632015	+0.04	- /1	+0.15	0.06/6	+0.29	0.06/15	+0.28	0.03/4	+0.07	0.06/12	-0.04	0.10/ 9	-0.05	- /1	
16233741-2638238	-0.09	0.23/6	-0.12	0.23/6	+0.22	0.09/13	+0.27	0.15/5	-0.16	0.18/12	-0.13	0.10/ 7	-0.23	- /1	
16234085-2631215	-0.05	- /1	+0.02	0.06/6	+0.23	0.06/14	+0.25	0.07/5	-0.05	0.04/12	-0.15	0.14/ 6	-0.16	- /1	
16234268-2631209	-0.01	0.22/5	-0.04	0.22/5	+0.30	0.07/10	+0.30	0.10/5	-0.01	0.10/ 4	-0.10	0.09/ 6	-0.09	- /1	
16234740-2631463	-0.04	- /1	-0.01	0.06/6	+0.25	0.04/13	+0.27	0.12/5	-0.01	0.08/13	-0.15	0.10/ 7	-0.12	- /1	
16235375-2634426	-0.12	- /1	+0.04	0.04/6	+0.23	0.05/16	+0.25	0.11/5	-0.01	0.08/13	-0.15	0.10/ 8	-0.09	- /1	
16240858-2624552	-0.09	- /1	+0.00	0.06/6	+0.23	0.06/15	+0.27	0.10/5	-0.06	0.07/12	-0.15	0.10/ 6	-0.12	- /1	
16231672-2634279	-0.05	- /1	+0.01	0.05/6	+0.24	0.05/15	+0.27	0.07/5	-0.03	0.08/13	-0.14	0.14/ 6	-0.13	- /1	
16232114-2631598	+0.16	0.07/6	+0.13	0.07/6	+0.32	0.08/14	+0.30	0.02/4	-0.01	0.07/ 9	-0.05	0.06/ 7	+0.03	0.05/2	
16232988-2631490	-0.12	- /1	-0.02	0.06/6	+0.21	0.05/16	+0.28	0.10/5	-0.08	0.07/13	-0.15	0.08/ 6	-0.12	- /1	
16233020-2633241	+0.06	0.08/5	+0.02	0.08/5	+0.23	0.05/12	+0.29	0.16/5	-0.10	0.22/12	-0.11	0.17/ 6	-0.16	- /1	
16233067-2629390	-0.10	0.14/6	-0.13	0.14/6	+0.25	0.06/14	+0.27	0.17/5	-0.10	0.21/10	-0.11	0.10/ 6	-0.11	- /1	
16233667-2630397	-0.04	- /1	-0.01	0.07/6	+0.22	0.04/15	+0.29	0.13/5	-0.04	0.10/13	-0.14	0.11/ 6	-0.07	- /1	
16233846-2629235	-0.11	- /1	-0.02	0.03/6	+0.23	0.07/15	+0.30	0.14/5	-0.07	0.07/12	-0.17	0.09/ 8	-0.14	- /1	
mean	-0.04		+0.01		+0.25		+0.28		-0.05		-0.12		-0.10		
±	0.02		0.02		0.01		0.01		0.01		0.01		0.01		
rms	0.07		0.07		0.03		0.03		0.05		0.04		0.06		
NGC 2808															
09120665-6450253	+0.03	0.05/6	+0.00	0.05/6	+0.20	0.07/14	+0.24	0.11/5	-0.11	0.09/13	-0.10	0.12/8	-0.12	0.02/2	
09120251-6451001	-0.03	- /1	-0.05	0.06/6	+0.18	0.07/14	+0.13	0.11/5	-0.12	0.05/11	-0.11	0.13/7	-0.12	0.01/2	
09120213-6452243	+0.04	0.05/6	+0.01	0.05/6	+0.14	0.06/13	+0.22	0.13/5	-0.14	0.11/12	-0.16	0.09/7	-0.10	0.07/2	
09114655-6452144	-0.08	- /1	+0.01	0.09/5	+0.15	0.08/15	+0.20	0.13/5	-0.07	0.09/13	-0.11	0.13/6	-0.14	- /1	
09122027-6448450	-0.15	- /1	+0.02	0.05/6	+0.17	0.05/15	+0.24	0.11/5	-0.12	0.04/12	-0.12	0.10/8	-0.07	0.02/2	
09123016-6454129	-0.09	- /1	+0.06	0.03/5	+0.23	0.09/16	+0.32	0.11/4	-0.07	0.07/12	-0.09	0.08/7	-0.05	- /1	
09120852-6449107	+0.12	0.06/6	+0.08	0.06/6	+0.24	0.09/14	+0.34	0.09/5	-0.04	0.10/13	-0.07	0.10/7	-	- /0	
mean	-0.02		+0.02		+0.19		+0.24		-0.10		-0.11		-0.10		
±	0.03		0.02		0.01		0.03		0.01		0.01		0.01		
rms	0.09		0.04		0.04		0.07		0.03		0.03		0.03		

Table 5: Derived chemical abundances for Fe, Co, Ni, Zn, Y, and Ce in M 4 and NGC 2808 AGBs.

ID (2MASS)	[Fe/H] I	rms/#	[Fe/H] II	rms/#	[Co/Fe]	rms/#	[Ni/Fe]	rms/#	[Zn/Fe]	rm/#	[Y/Fe] II	rms/#	[Ce/Fe] II	rms/#
M 4														
16233142-2633110	-1.18	0.08/75	-1.14	0.09/6	-0.03	0.02/4	-0.01	0.08/28	+0.19	- /1	+0.26	0.16/4	+0.13	-/1
16233477-2631349	-1.22	0.08/68	-1.20	0.08/8	+0.07	- /1	+0.01	0.10/28	+0.09	- /1	+0.39	0.09/4	+0.31	-/1
16233535-2632225	-1.26	0.08/88	-1.24	0.10/8	-0.07	0.06/4	-0.03	0.08/30	+0.16	- /1	+0.29	0.18/3	+0.17	-/1
16233614-2632015	-1.12	0.07/92	-1.08	0.07/9	-0.05	0.06/4	-0.03	0.06/32	+0.19	- /1	+0.32	0.15/4	+0.09	-/1
16233741-2638238	-1.22	0.08/67	-1.19	0.18/9	-0.05	0.05/3	-0.03	0.10/24	+0.34	0.07/2	+0.23	0.11/4	+0.01	-/1
16234085-2631215	-1.18	0.09/84	-1.15	0.08/8	-0.07	0.09/4	-0.02	0.07/31	+0.25	- /1	+0.36	0.15/3	+0.35	-/1
16234268-2631209	-1.07	0.09/45	-1.04	0.14/8	-0.11	- /1	-0.01	0.08/14	+0.24	- /1	+0.38	0.06/4	+0.25	-/1
16234740-2631463	-1.28	0.08/89	-1.25	0.10/9	-0.03	0.04/4	-0.02	0.06/30	+0.31	0.18/2	+0.21	0.14/3	+0.15	-/1
16235375-2634426	-1.21	0.08/87	-1.18	0.07/9	-0.03	0.06/4	-0.02	0.07/28	+0.23	- /1	+0.27	0.13/4	+0.11	-/1
16240858-2624552	-1.27	0.07/85	-1.24	0.08/9	-0.06	0.08/4	-0.04	0.06/30	+0.20	0.03/2	+0.16	0.12/4	+0.07	-/1
16231672-2634279	-1.24	0.08/86	-1.20	0.07/9	-0.07	0.05/3	-0.02	0.07/30	+0.17	- /1	+0.25	0.11/4	+0.13	-/1
16232114-2631598	-1.14	0.07/67	-1.11	0.07/9	-0.03	0.08/2	+0.00	0.09/28	+0.16	- /1	+0.33	0.13/4	+0.18	-/1
16232988-2631490	-1.28	0.07/83	-1.25	0.08/9	-0.04	0.05/4	-0.04	0.07/31	+0.33	0.15/2	+0.28	0.16/4	+0.13	-/1
16233020-2633241	-1.19	0.07/66	-1.15	0.10/7	-0.02	0.04/3	-0.01	0.07/27	+0.44	0.07/2	+0.21	0.15/3	+0.08	-/1
16233067-2629390	-1.18	0.07/61	-1.15	0.15/9	-0.02	0.05/3	+0.01	0.11/23	+0.30	0.01/2	+0.14	0.09/4	+0.02	-/1
16233667-2630397	-1.24	0.08/82	-1.21	0.07/9	-0.04	0.05/4	-0.01	0.07/27	+0.23	- /1	+0.30	0.12/4	+0.06	-/1
16233846-2629235	-1.17	0.08/78	-1.14	0.06/8	-0.04	0.02/3	-0.03	0.09/30	+0.16	- /1	+0.17	0.10/4	+0.13	-/1
mean	-1.20		-1.17		-0.04		-0.02		+0.23		+0.27		+0.14	
±	0.01		0.01		0.01		0.01		0.02		0.02		0.02	
rms	0.06		0.06		0.04		0.01		0.08		0.07		0.09	
NGC 2808														
09120665-6450253	-1.30	0.07/68	-1.27	0.06/9	-0.02	0.07/3	-0.07	0.07/25	-0.01	- /1	-0.13	0.15/3	-0.17	-/1
09120251-6451001	-1.31	0.08/71	-1.24	0.07/9	-0.17	0.07/2	-0.10	0.09/26	+0.13	0.22/2	-0.16	0.06/4	-0.11	-/1
09120213-6452243	-1.30	0.07/67	-1.27	0.05/8	-0.12	0.18/2	-0.07	0.13/26	+0.03	- /1	-0.04	0.12/3	-0.13	-/1
09114655-6452144	-1.25	0.08/81	-1.21	0.06/9	-0.15	0.00/3	-0.13	0.09/27	+0.08	- /1	-0.01	0.14/3	-0.15	-/1
09122027-6448450	-1.32	0.09/81	-1.29	0.06/9	-0.17	0.01/4	-0.10	0.09/25	+0.14	- /1	-0.03	0.10/4	-0.06	-/1
09123016-6454129	-1.20	0.08/75	-1.17	0.09/9	-0.13	0.04/2	-0.12	0.08/23	+0.21	0.16/2	+0.11	0.10/4	+0.08	-/1
09120852-6449107	-1.19	0.08/80	-1.15	0.07/9	-0.06	0.01/3	-0.04	0.11/19	+0.20	0.04/2	+0.07	0.16/3	-	-/0
mean	-1.27		-1.23		-0.12		-0.09		+0.11		-0.03		-0.09	
±	0.02		0.02		0.02		0.01		0.03		0.04		0.04	
rms	0.05		0.05		0.05		0.03		0.08		0.09		0.08	

5. Summary and conclusions

We provide a photometric and spectroscopic investigation of multiple populations along the AGB of the Galactic GCs NGC 2808 and M 4. Our study is based on: *(i)* high-resolution spectroscopy from FLAMES@VLT; *(ii)* multi-wavelength photometry from the *HST* UV survey of Galactic GCs and from ground-based telescopes; and *(iii)* proper motions derived by combining stellar positions from Gaia DR1 and positions derived from images collected with WFI@MPI2.2m telescope.

In NGC 2808 we have identified three main stellar populations of AGB-1, AGB-2, and AGB-3 stars that populate three AGB sequences in the m_{F438W} vs. $C_{F275W,F336W,F438W}$ pseudo-CMD and in the $\Delta_{CF275W,F336W,F438W}$ vs. $\Delta_{F275W,F814W}$ pseudo two-color diagram, or ‘chromosome map’. The three populations of AGB-1, AGB-2, and AGB-3 stars include the 41%, 32%, and 27% of the total number of AGB stars and have different O, Na, Mg, and Al abundances. This evidence of multiple populations of AGB stars in NGC 2808 adds to the recent finding by Wang et al. (2016) based on the distribution of Na in the same cluster. By combining information from this paper and from the literature we followed multiple stellar populations along the different evolutionary phases, from the MS to the HB and AGB of NGC 2808.

Recent papers show that NGC 2808 hosts five main populations, namely A–E, that have been detected along the MS and the RGB by using multi-wavelength photometry and correspond to stellar populations with different helium and light-element abundance (Milone et al. 2015a; Carretta 2015). Unfortunately, there are no spectroscopic studies on population-A stars. On the AGB, we find in this paper that AGB-1 stars mostly correspond to population B, while AGB-2 stars are the progeny of the RGB-C. Population-D stars are enhanced in helium up to $Y \sim 0.32$ and have low oxygen and high sodium abundance. We have shown that population-D stars climb the AGB and define the sequence of AGB-3 stars in the m_{F438W} vs. $C_{F275W,F336W,F438W}$ pseudo-CMD.

We did not find any spectroscopic evidence for population-E stars with extreme helium and light-element abundance along the AGB although the small number of analyzed stars prevents us from strong conclusions on the basis of spectroscopy only. However, this idea is strengthened by the analysis of the ‘chromosome map’ of AGB stars: by comparing the relative numbers of stars along the distinct AGBs and RGBs we concluded that the fraction of AGB-3 stars with respect to the total number of AGB stars is not consistent with the presence of population-E along the AGB. The possibility that population-E stars avoid the AGB phase is further supported by the presence of evolved stars that are clearly visible in the m_{F275W} vs. $m_{F275W} - m_{F814W}$ CMD of Figure 2 (blue diamonds) and that have been interpreted by Castellani et al. (2003) as “AGB manque” stars. Since population-E stars

have extreme helium abundance ($Y \sim 0.38$, D’Antona et al. 2005; Piotto et al. 2007; Milone et al. 2015a), our findings support the prediction from stellar evolution that He-rich stars in stellar populations avoid the AGB phase and evolve as AGB-manque’ stars (e.g. Greggio & Renzini 1990; D’Cruz et al. 2000; Brown et al. 2001; Moehler et al. 2004; Gratton et al. 2010; Chantereau et al. 2016).

Specifically, we note that NGC 2808 is considered a quite young GC (age= 11.5 ± 0.75 Gyr, Dotter et al. 2010; Milone et al. 2014). The lack of stars with extreme helium abundance along the AGB of NGC 2808 would be in agreement with the conclusion by Charbonnel & Chantereau (2016), who predict that the internal AGB helium spread of a GC with $[\text{Fe}/\text{H}] = -1.15$ and age= 11.5 is smaller than $\Delta Y \sim 0.09$. The GC M 4 has similar metallicity and age (12.50 ± 0.50 Gyr) as NGC 2808 (although NGC 2808 seems slightly younger, Marín-Franch et al. 2009). In contrast, in the context of multiple populations, M 4 looks much less complex than NGC 2808. This cluster hosts two main populations of stars with different C, N, O, Na abundance that have been observed along the MS and RGB (e.g. Marino et al. 2008; Piotto et al. 2015). Na-poor/O-rich stars are slightly enhanced in helium by $\Delta Y \sim 0.02$ (Nardiello et al. 2015) with respect to the primordial value and populate the red HB while the blue HB host stars more-depleted in oxygen and with higher in sodium (Marino et al. 2011). Despite the possible presence of systematics between the abundances of AGB and RGB stars, we find that the chemical abundances dispersions of AGB stars in M 4 are not consistent with a simple stellar population and provide both photometric and spectroscopic evidence that stars belonging to different populations ascend the AGB of this cluster.

In conclusion, while in NGC 2808 the extremely He-rich (Na-rich, O-poor) population of the RGB very likely misses the AGB phase, in M 4 we do not find any strong evidence for a lack of some of the RGB populations on the AGB. Except for the lack of the extremely He-enhanced population of NGC 2808, the number ratios of second population AGB stars are similar to those observed on the RGB in both GCs. These results suggest that only a high level of He enrichment, like in the extreme population of NGC 2808, is able to make a star avoiding the AGB phase. At a given metallicity and age, He seems to be the main parameter controlling evolution towards the AGB.

We are grateful to the referee for several suggestion that have improved the quality of this manuscript. We thank P. B. Stetson who has kindly provided us the ground-based photometric catalogs of M 4 and NGC 2808, Ben MacClean for supplying positions of his M 4 AGB stars to enable a cross-match with our sample, and Simon Campbell for useful discussion. This work has been supported by the Australian Research Council (grants DE160100851, DE150101816, DP150100862, FT140100554, FL110100012).

REFERENCES

- Anderson, J., Bedin, L. R., Piotto, G., Yadav, R. S., & Bellini, A. 2006, *A&A*, 454, 1029
- Anderson, J., Sarajedini, A., Bedin, L. R., et al. 2008, *AJ*, 135, 2055
- Ballester, P., Modigliani, A., Boitquin, O., et al. 2000, *The Messenger*, 101, 31
- Bedin, L. R., Piotto, G., Zoccali, M., et al. 2000, *A&A*, 363, 159
- Bergemann, M., Lind, K., Collet, R., Magic, Z., & Asplund, M. 2012, *MNRAS*, 427, 27
- Brown, T. M., Sweigart, A. V., Lanz, T., Landsman, W. B., & Hubeny, I. 2001, *ApJ*, 562, 368
- Carretta, E., Bragaglia, A., Gratton, R. G., et al. 2006, *A&A*, 450, 523
- Campbell, S. W., D’Orazi, V., Yong, D., et al. 2013, *Nature*, 498, 198
- Carretta, E., Bragaglia, A., Gratton, R. G., et al. 2009, *A&A*, 505, 117
- Carretta, E. 2014, *ApJ*, 795, L28
- Carretta, E. 2015, *ApJ*, 810, 148
- Castelli, F., & Kurucz, R. L. 2004, arXiv:astro-ph/0405087
- Chantereau, W., Charbonnel, C., & Meynet, G. 2016, *A&A*, 592, A111
- Charbonnel, C., & Chantereau, W. 2016, *A&A*, 586, A21
- D’Antona, F., Bellazzini, M., Caloi, V., et al. 2005, *ApJ*, 631, 868
- D’Cruz, N. L., O’Connell, R. W., Rood, R. T., et al. 2000, *ApJ*, 530, 352
- Dekker, H., D’Odorico, S., Kaufer, A., Delabre, B., & Kotzlowski, H. 2000, *Proc. SPIE*, 4008, 534
- Dotter, A., Sarajedini, A., Anderson, J., et al. 2010, *ApJ*, 708, 698
- Dotter, A., Ferguson, J. W., Conroy, C., et al. 2015, *MNRAS*, 446, 1641
- Gratton, R. G., Carretta, E., Eriksson, K., & Gustafsson, B. 1999, *A&A*, 350, 955
- Gratton, R. G., D’Orazi, V., Bragaglia, A., Carretta, E., & Lucatello, S. 2010, *A&A*, 522, A77

- Gratton, R. G., Carretta, E., & Bragaglia, A. 2012, *A&A Rev.*, 20, 50
- Greggio, L., & Renzini, A. 1990, *ApJ*, 364, 35
- Gruyters, P., Casagrande, L., Milone, A. P., et al. 2017, arXiv:1704.08878
- Harris, W. E. 1996, *VizieR Online Data Catalog*, 7195,
- Ivans, I. I., Sneden, C., Kraft, R. P., et al. 1999, *AJ*, 118, 1273
- Ivans, I. I., Kraft, R. P., Sneden, C., et al. 2001, *AJ*, 122, 1438
- Johnson, C. I., McDonald, I., Pilachowski, C. A., et al. 2015, *AJ*, 149, 71
- Kausch, W., Noll, S., Smette, A., et al. 2015, *A&A*, 576, A78
- Kraft, R. P. 1994, *PASP*, 106, 553
- Lapenna, E., Mucciarelli, A., Ferraro, F. R., et al. 2015, *ApJ*, 813, 97
- Lapenna, E., Lardo, C., Mucciarelli, A., et al. 2016, *ApJ*, 826, L1
- Lardo, C., Salaris, M., Savino, A., et al. 2017, *MNRAS*, 466, 3507
- Lee, J.-W., Kang, Y.-W., Lee, J., & Lee, Y.-W. 2009, *Nature*, 462, 480
- Lind, K., Asplund, M., Barklem, P. S., & Belyaev, A. K. 2011, *A&A*, 528, A103
- Lind, K., Bergemann, M., & Asplund, M. 2012, *MNRAS*, 427, 50
- Lindegren, L., Lammers, U., Bastian, U., et al. 2016, *A&A*, 595, A4
- MacLean, B. T., Campbell, S. W., De Silva, G. M., et al. 2016, *MNRAS*, 460, L69
- Marín-Franch, A., Aparicio, A., Piotto, G., et al. 2009, *ApJ*, 694, 1498
- Marino, A. F., Villanova, S., Piotto, G., et al. 2008, *A&A*, 490, 625
- Marino, A. F., Villanova, S., Milone, A. P., et al. 2011, *ApJ*, 730, L16
- Marino, A. F., Milone, A. P., Przybilla, N., et al. 2014, *MNRAS*, 437, 1609
- McLachlan, G., & Peel, D. 2000, *Finite Mixture Models* (New York: Wiley)
- Milone, A. P., Piotto, G., Bedin, L. R., et al. 2012, *A&A*, 540, A16
- Milone, A. P., Marino, A. F., Piotto, G., et al. 2013, *ApJ*, 767, 120

- Milone, A. P., Marino, A. F., Bedin, L. R., et al. 2014, MNRAS, 439, 1588
- Milone, A. P. 2015, MNRAS, 446, 1672
- Milone, A. P., Marino, A. F., Piotto, G., et al. 2015a, ApJ, 808, 51
- Milone, A. P., Marino, A. F., Piotto, G., et al. 2015b, MNRAS, 447, 927
- Milone, A. P., Piotto, G., Renzini, A., et al. 2017, MNRAS, 464, 3636
- Moehler, S., Sweigart, A. V., Landsman, W. B., Hammer, N. J., & Dreizler, S. 2004, A&A, 415, 313
- Monelli, M., Milone, A. P., Stetson, P. B., et al. 2013, MNRAS, 431, 2126
- Nardiello, D., Piotto, G., Milone, A. P., et al. 2015a, MNRAS, 451, 312
- Nardiello, D., Milone, A. P., Piotto, G., et al. 2015b, A&A, 573, A70
- Norris, J., Cottrell, P. L., Freeman, K. C., & Da Costa, G. S. 1981, ApJ, 244, 205
- Pasquini, L., Avila, G., Allaert, E., et al. 2000, Proc. SPIE, 4008, 129
- Piotto, G., Bedin, L. R., Anderson, J., et al. 2007, ApJ, 661, L53
- Piotto, G., Milone, A. P., Anderson, J., et al. 2012, ApJ, 760, 39
- Piotto, G., Milone, A. P., Bedin, L. R., et al. 2015, AJ, 149, 91
- Simioni, M., Milone, A. P., Bedin, L. R., et al. 2016, MNRAS, 463, 449
- Smette, A., Sana, H., Noll, S., et al. 2015, A&A, 576, A77
- Smith, G. H., & Norris, J. E. 1993, AJ, 105, 173
- Snedden, C. A. 1973, Ph.D. Thesis,
- Stetson, P. B. 1987, PASP, 99, 191
- Stetson, P. B. 1994, PASP, 106, 250
- Stetson, P. B. 2000, PASP, 112, 925
- Stetson, P. B., Braga, V. F., Dall’Ora, M., et al. 2014, PASP, 126, 521
- Villanova, S., & Geisler, D. 2011, A&A, 535, A31

Villanova, S., Geisler, D., Piotto, G., & Gratton, R. G. 2012, *ApJ*, 748, 62

Wang, Y., Primas, F., Charbonnel, C., et al. 2016, *A&A*, 592, A66